Strong Coupling of an Emitter with Absorbing Matter: A Regime for Enhancement of Light Emission

Kritika Jain and Murugesan Venkatapathi[*]

Computational and Statistical Physics Laboratory, Indian Institute of Science, Bangalore 560012, India

This work shows that, counterintuitively, adding extremely small (< 10 nm in dimension) fully absorbing metal nanoparticles to a material can notably enhance its light emission. It also shows that the mystery behind the unexpected large enhancements in surface-enhanced Raman spectroscopy, even greater than a factor of 10^{10}, is the tunneling out of photons from the strongly absorbing metal surface. Dynamics in a strongly coupled emitter-matter quantum system demands such behavior in the case of limiting small metal nanoparticles and proximal metal surfaces. This effect can be exploited further in light generation, optical sensing, and radiative heat transfer.

I. INTRODUCTION

Spontaneous emission is well understood as the function of vacuum and surrounding matter. The strong vacuum-coupling regime becomes relevant when only a few optical states (modes) of vacuum are available for the emission, as in a microcavity. In many applications, such emitter-vacuum coupling in a cavity and the resulting dynamics are not of interest. Alternatively, in the weak vacuum-coupling regime, probability of spontaneous emission is altered by modifying the *density* of optical states due to the surrounding matter. Increasing the density of radiative states relative to the nonradiative (absorbing) states using appropriate matter placed near emitters can result in significant gains in power and even efficiency of emission [1–8]. A metal nanoparticle only a few nanometers in dimension is fully absorbing, and while this dissipation increases proportionally with its volume, its scattering increases as the square of its volume. The strong elastic scattering of larger plasmonic nanoparticles 50–200 nm in dimension, when separated from emitters by distances on the order of their dimensions, is associated with a larger increase in the density of radiative states. This idea of exploiting the interaction of emitters with cavities and proximal matter is broadly referred to as Purcell enhancement [9]. Here the radiative and nonradiative states of the excited nanoparticle appear as a simple addition over corresponding states available to the isolated emitter in vacuum, and one may call it the weak matter-coupling regime of emission.

Recently, inhibited quenching of emission observed near metal nanoparticles less than 15 nm in dimension, and the anomalous gains observed in resonant and off-resonant

cases of the smallest metal nanoparticles [10–16], contradicts this current understanding. Our work points to a break down of conventional theory of local density of optical states when dynamics of fluctuations between an emitter and proximal matter play a significant role in the emission process. This effect manifests in a wider range of spatial separations relative to the small size of these nanoparticles. Thus it can reduce the volume of metal inclusions used in exploiting the Purcell effect for bulk materials, and has significant practical advantages where maintaining appropriate distances between a large number of nanoparticles and emitters is a challenge.

We also show that widely used optical sensing techniques such as surface-enhanced Raman spectroscopy (SERS) exhibit gains even larger than 10^{10} in magnitude [17–24] primarily due to this effect discussed in this work, which otherwise would be restricted to a factor of 10^3. In many cases of sensing fluorescence and Raman signals, near-field enhancement of incident radiation exciting the emitter, accompanies a possible enhancement of its emission. Typically, a metallic surface or a larger nanostructure hosts smaller (sharper) nano features that result in this near-field enhancement of exciting radiation [see Fig. 1(a)]. By conventional theory, this surface adds nonradiative states significantly more than radiative states for emission. But observed factors of enhancement due to a metallic surface are much greater than the combined amplification possible due to relative increase in exciting radiation and density of radiative states, for both resonant and off-resonant emissions. The unexpected large enhancements of Raman signals typically observed has lead to the proposal of provisional mechanisms [25–27] that implicitly ignore the large absorption of metals as required in conventional electrodynamics. Hence, this divergence of
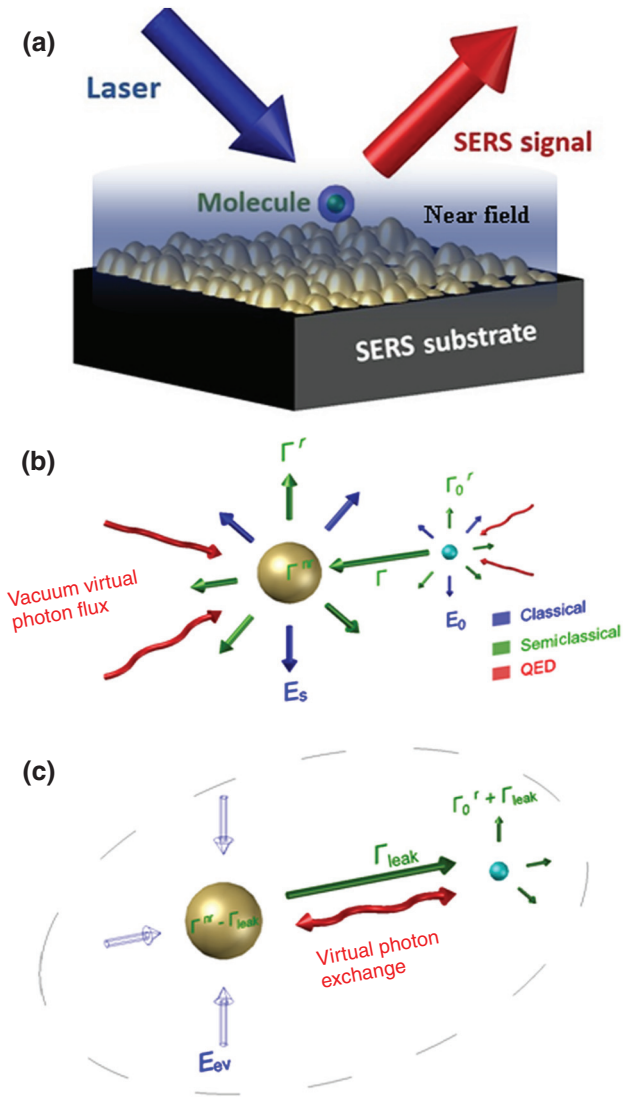
———————
*murugesh@iisc.ac.in

FIG. 1. (a) A rough metal surface used to enhance Raman signals in SERS. (b) Conventional models of emitter (cyan) interacting with matter (yellow): work done on an emitting dipole by the scattered field ($\mathbf{E}_s$) of metal nanoparticle is a classical first approximation of modified emission; semiclassical evaluations of the additional decay rates Γ (with superscripts "r" for radiative and "nr" for nonradiative, and subscripts "o" for parameters of the isolated emitter) include optical states of the excited metal nanoparticle; QED predicts an increase of vacuum fluctuations coupled to the emitter due to a nanoparticle that scatters strongly. (c) Additional components involved in the case of a strong coupling of an emitter with absorbing matter where evanescent fields ($\mathbf{E}_{ev}$) are dominant.

experiments from theory has also been attributed to a *chemical* enhancement of unknown origin [28]. On the other hand, varying chemical properties of dyes introduce variations of at most an order of magnitude in the surface-enhanced Raman signals [29,30]. Further, measurements resolved with a varying distance from the nanostructure [17,18] have shown that this divergence of

SERS enhancements from the theory may have a longer range than expected in a chemical effect.

In both strong vacuum-coupling [31–35] and recently indicated strong matter-coupling [36,37] regimes of emission, experiments establish the splitting of the emitted energy spectrum due to Rabi oscillations. This reversible exchange of the excitation between two oscillators, and the two possible modes of the coupled system, are observable when dissipation in the two oscillators is relatively negligible. But a significant unknown is the degree of dissipation possible when we have such a strong coupling between an emitter and absorbing matter. We show that only when the probability of dissipation and radiation by the excited metal nanostructure (decay rate) is significantly larger than the probability of exchange of this excitation back to the emitter (Rabi frequency), conventional partition of optical states holds. Otherwise, an inhibited dissipation results in an equivalent increase in the emitter's coupling to vacuum. Such a large increase in radiative states at the cost of non-radiative states is predicted for limiting small dimensions of a metal nanoparticle, and a metal structure separated by only a few nanometers from the emitter.

From a classical electrodynamics point of view, the immediate near-field zone of an excited metallic structure has a relatively large component of evanescent fields, and in the dissipation by extremely small metal nanoparticles this strongly evanescent zone can be significantly larger than the particle. Originally thought to have no physical significance, these fields are found to play a dominant role in phenomena ranging from tunneling across a thin potential barrier [38–40], to the large fluctuation-driven heat transfer very near a surface [41,42]. The emitter coupled to an evanescent field of a metal structure can be re-excited by its emitted photon that would have otherwise dissipated in the metal. It is reasonable to postulate that this inhibited dissipation in the metal should be accompanied by other quantum effects represented by a superposition of such virtual re-excitations, including an increase of coherence and tunneling out of photons from the metal structure. But it is nontrivial to evaluate evanescent fields and these quantum effects as such, and our model of strong coupling described later provides a comprehensive approach [schematics in Figs. 1(b) and 1(c)]. Here we have an anomalous case of significant proximal emission, where conventional theory predicts large nonradiative absorption and a near-zero probability of classical scattering of the emitted photon by the nanostructure. Hence, though very different in scale and origin, this behavior has an interesting analogy in the quantum tunneling of particles that manifests as Hawking radiation near an otherwise fully ingesting black hole [43].

II. METHODS

Here we introduce the required corrections in the conventional density of optical states when an emitter is

strongly coupled to absorbing matter. As a result, a significant fraction of the nonradiative component of the dipole mode of a nanostructure can manifest as a radiative component. We first briefly refer to known methods used to evaluate the modified self-energy of a point dipole in an inhomogeneous medium, and relegate the details of required Green dyads to the Appendix. This problem may not have closed-form analytical solutions in general, and a quasistatic solution in the long-wavelength limit has typically been preferred [44]. This may result in errors in the estimated energy shifts [45], and in an underestimation of nonradiative decay rates in metal nanostructures [46]. Hence, we resort to more computationally intensive approaches to include retardation for finite wavelengths, and evaluate the variables in the proposed theory described below. But we emphasize that the divergence of experiments from conventional theory is evident even in calculations using first approximations. Analytic evaluations using single-dipole approximation of these smaller metal nanoparticles, and a quasistatic approximation of a metal surface for the case of SERS measurements, are also presented in the Supplemental Material [47].

The additional decay rate due to the metallic structure is given by the imaginary part of its self-energy contribution Σ, i.e., $\Gamma = -2 \, \mathrm{Im}(\Sigma)$; these units reflect a normalization by the reduced Planck constant as in Eq. (4) describing the real part. The contribution of the nanostructure to self-energy of an emitter at $\mathbf{r_o}$ is given by

$$\Sigma(\omega) = \frac{-2\pi q^2 \omega}{mc^2} \mathbf{e}_o \cdot \mathbf{G}(\mathbf{r_o}, \mathbf{r_o}; \omega) \cdot \mathbf{e}_o \tag{1}$$

and the above can be integrated over polarization vectors $\mathbf{e}_o$, and over frequency ω with the relative spectral density of the free-space emitter in the case of broad-band emission. Here q is the oscillating charge, m is its mass, and c is the speed of light. Γ_0^r and Γ_0^{nr} are known radiative and nonradiative decay rates of the isolated emitter adding to Γ_o. The total radiative and nonradiative parts are a sum of the free space and metallic components as below

$$\Gamma_{\mathrm{total}}^r = \Gamma_0^r + \Gamma^r. \tag{2}$$

Note that a dipole oscillator with an energy of one quantum represents the emitter as a two-level system in this weak vacuum-coupling regime. It is convenient to drop charge, mass, and amplitude of the oscillator and normalize all self-energy components by Γ_0^r for evaluations, where $\Gamma_0^r = 2\sqrt{\epsilon_o}\mu^2 k^3/3\hbar$ and μ is the electric dipole moment of the emitter; k, ϵ_o, and $\hbar$ are the wave number, free-space permittivity, and reduced Planck constant.

$$\Gamma_{\mathrm{total}}^{nr} = \Gamma_0^{nr} + \Gamma^{nr}, \tag{3}$$

where Γ^r and Γ^{nr} are additional radiative and nonradiative decay rates of the emitter in the presence of metal

nanostructure, adding to the total metallic contribution Γ. The optical theorem for a point source establishes that the evaluated self-interaction of an emitter due to a proximal body represents the total radiative (scattering) and nonradiative (absorption) states of the body. The spatial reflection symmetry of the free space and the scattering component of the Green dyads, allows us to equally interpret this perturbation to self-energy as additional action of vacuum on the emitter due to the presence of the body. The modified emission can thus be inferred as the increase in vacuum fluctuations coupled to emitter, due to the body. The real part of self-energy in Eq. (1) represents shifts from the isolated emitter's resonance [44], and the energy split between the two modes of the strongly coupled system is given by twice this value.

$$2\hbar|\mathrm{Re}(\Sigma)| = \Delta E. \tag{4}$$

More importantly, in the rotating wave approximation $(|\mathrm{Re}(\Sigma)| \ll \omega)$, $\Delta E/\hbar$ is the rate of exchange of excitation between emitter and nanostructure, i.e., the frequency of Rabi oscillations. This exchange in the form of emission and absorption of virtual photons is accompanied by the creation and annihilation of virtual plasmons in the metal particle. Typically, $\Gamma \gg \Delta E/\hbar$ resulting in a negligible probability of a virtual plasmon annihilation in metals, and this regime is also irrelevant for dielectric materials where Γ^{nr} is negligible. But in the case of the smallest metal nanoparticles, decay rates and frequency of Rabi oscillations are comparable (see Figs. 6 and 7 in the Appendix). Even for an emitter close to a large metallic nanostructure the above inequality is significantly weak. Note that this would replace absorption with an equivalent generation of photons by virtual plasmon annihilation, and is especially significant for the dipole mode of a nanostructure that represents most of its coupling to vacuum modes. These fluctuations of the dipole mode should not be distinguished from its scattering of virtual photons from vacuum. Only the latter contribution of elastic scattering is included in the increase of radiative states in conventional theory. Thus, the following extension of the local density of optical states becomes necessary.

First, we assume the memoryless probability *density* function in time τ for the real decay of plasmon, i.e., $\Gamma e^{-\Gamma \tau}$. The typical case of integration of this probability density in the interval [0,t], and taking its complement, gives the probability of its excited state as $e^{-\Gamma t}$ for all t. But here we restrict it to the interval of a Rabi oscillation as shown below

$$\mathcal{P}_{\mathrm{real}} = \int_{\tau=0}^{\tau=\hbar/\Delta E} \Gamma e^{-\Gamma \tau} d\tau. \tag{5}$$

Since the virtual decay of plasmon is due to every Rabi oscillation between the emitter and the nanoparticle, we

use the complement of $\mathcal{P}_{\text{real}}$ as the probability of generation of virtual photons. This probability of creation and annihilation of virtual plasmons can be non-negligible and thus given by

$$\mathcal{P}_{\text{virtual}} = 1 - \mathcal{P}_{\text{real}} = e^{-\hbar\Gamma/\Delta E}. \tag{6}$$

The coupling of nanostructure to vacuum modes is primarily represented by its dipole mode contributions, which are numbered "1" in the subsequent part of this section. This dynamics can only marginally reduce the absorption of higher-order modes, which have zero dipole moments and are coupled weakly to vacuum modes. These higher-order nondipolar modes can remain uncorrected in this work, as we are interested only in limiting small nanospheres and image dipoles due to surfaces. We can not distinguish these additional fluctuations of the dipole mode of nanostructure from that of vacuum. Its effect on the nonradiative and radiative rates of the emitter is trivially evaluated as below. Let

$$\Gamma_{\text{leak}} = e^{-\hbar\Gamma/\Delta E} \times \Gamma_1^{nr}. \tag{7}$$

This rate accounts for the vanishing of the nonradiative absorption of the dipole mode and its appearance as a stronger radiative mode. The effective decay rates thus become

$$\Gamma_{\text{eff}}^r = \Gamma_0^r + \Gamma^r + \Gamma_{\text{leak}} \tag{8}$$

and

$$\Gamma_{\text{eff}}^{nr} = \Gamma_0^{nr} + \Gamma^{nr} - \Gamma_{\text{leak}}. \tag{9}$$

The observed quantum efficiency is then

$$Q = \frac{\Gamma_{\text{eff}}^r}{\Gamma_{\text{eff}}^r + \Gamma_{\text{eff}}^{nr}}. \tag{10}$$

Note the strong effect even a relatively small $\mathcal{P}_{\text{virtual}}$ has on radiative rates and the emitted power, in the case of a proximal large metallic nanostructure or surface dominated by nonradiative decay (i.e., $\Gamma_{\text{eff}}^r \gg \Gamma^r + \Gamma_0^r$). The quantum nature of interactions is salient in the corrections here, and it well represents broadly observed effects with different types of emitters and metal particles. Predictions can be weakly sensitive to a further quantization of the particle or emitter in special cases.

III. RESULTS AND DISCUSSION

Our goal in this section is to demonstrate the suggested effect, using known independent experimental observations of various types of optical emission, that seemed anomalous otherwise. Here we do not repeat the details of the preparation of materials, but they are summarized in our Supplemental Material [47] along with the exact location of experimental data points in the original papers.

The smaller nanoparticles can absorb light in the plasmonic range increasing nonradiative states notably, but have a negligible scattering efficiency and do not add to the density of radiative states. But they have been observed to increase rates of spontaneous emission from proximal emitters significantly more than theoretical evaluations, and in cases even notably increase their efficiency of emission in a direct contradiction with theory. First, we begin with some of the experiments of fluorescence and photoluminescence in materials with metal nanoparticles of limiting small sizes, referred to in Sec. 1 earlier. The exciting radiation is off resonant, and the limiting small absorbing nanoparticle does not significantly alter the intensity of the light exciting the emitter. The rates of radiative and nonradiative processes are estimated using independent life-time measurements in many cases, in addition to the measurement of gain in the photons emitted. The measured gains are relatively robust and repeatable, while the decay rate is more sensitive to any uncertainty in distances [47]. To compare, we present polarization averaged evaluations of both relative quantum efficiency and relative power of emission (Q and $Q\Gamma^r$ in the previous section), with respect to isolated emitters not interacting with metal nanostructures. The former represents the change in the probability of radiative decay of the excited emitter and is the minimum factor of enhancement expected. The latter also includes the maximum relative increase in ground-state population for emitters excited continuously. This maximum limit becomes relevant when robust emitters can be subjected to repeated excitation as in the case of SERS measurements.

Figure 2 presents the measured gains for varying separations of a low-efficiency emitter from a gold nanoparticle of 5-nm radius. The large gains in the observed emission and its contradiction with conventional semiclassical theory that predicts quenching, are clear. Whereas the proposed theory predicts these measurements reasonably well notwithstanding possible uncertainty in efficiency of the isolated emitters. Figure 3 presents experiments of quenched emission from two different types of emitters. Here the nanoparticles are marginally larger at 6.5-nm radii and the quenching in the experimental results is significantly less than the expected values of the conventional semiclassical theory. In contrast these experiments have a reasonable agreement with the predicted range of this extended theory for strong coupling. Note that weak quenching due to polymer molecules binding the emitter-nanoparticle system has not been included in both the theoretical models of relative emissions. Hence,
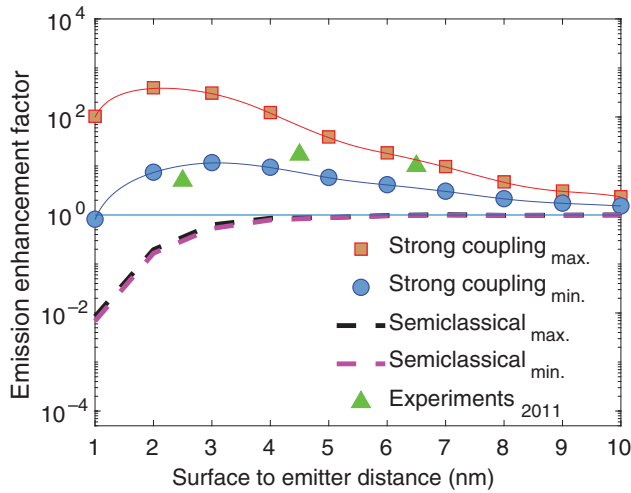
FIG. 2. Comparison of theoretical results and observed fluorescence: the minimum and maximum gains predicted are given by quantum efficiency and power radiated, normalized by the values of the isolated emitter; note log scale in the Y axis. Experimental data [11] is for a gold nanoparticle of radius 5 nm coated with a bipolymer and the peak emission wavelength is 830 nm with a $Q_o \approx 0.012$.
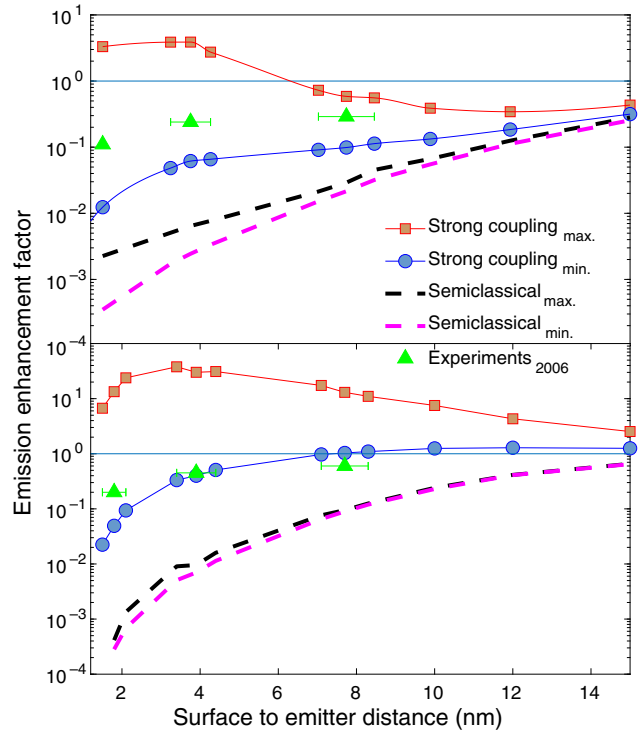

FIG. 3. Comparison of theoretical results and observed fluorescence: the minimum and maximum gains predicted are given by quantum efficiency and power radiated, normalized by the values of the isolated emitter; note log scale in the Y axis. Experimental data [12] is for gold nanoparticles of radius 6.5 nm. Top: $Q_o \approx 1$ and peak emission wavelength is 520 nm. Bottom: $Q_o \approx 0.37$ and peak emission wavelength is 580 nm.

theoretical predictions at the worst can only be a marginal overestimation of the experimental observations.

Multiple experiments by other researchers on even smaller gold nanoparticles using self-assembled films and monolayers with quantum-dot emitters, are summarized in Fig. 4. Note that for the smaller metal nanoparticles discussed in Figs. 2 and 4, the experiments present a direct contradiction; semiclassical theory predicts quenching while experiments report significant enhancements of emission. Monolayers with smaller separations of emitters and gold nanoparticles of a smaller radii of 1.75 nm, have larger divergence with conventional theory as expected (section on the left in Fig. 4). But the notable enhancement up to a factor of 3 for the emitters embedded in the films due to sparsely doped and well-separated 2.5-nm radii gold nanoparticles are equally unexpected (on the right in Fig. 4). In this section on the right, four experiments with nearly overlapping gain values are marked along with the predictions of theory. Our modified theory of the local density of optical states to include effects of strong coupling predicts these experiments reasonably well. One aspect of the experiments with limiting small metal nanoparticles of 1.75-nm radii, is the weak sensitivity to the number ratio of emitters and metal particles in the monolayer [48]. Possible collective behavior among emitters has been suggested in the presence of plasmonic nanoparticles [49], phonon interactions [50], and otherwise at low temperatures [51]. But these theoretical works involved long-wavelength approximations and neglected thermal effects; while other feeble indications of such collective behavior of emitters in the weak vacuum-coupling

regime are few [52–54]. Our studies on the weaker effects of such parameters of the monolayer will be presented elsewhere.

In the case of SERS, we summarize multiple observations to compare predictions of the proposed theory. These enhancements in Raman signals due to metallic nanostructures of various geometries are typically predicted by a power-4 rule that does not consider absorption by the metal, i.e., $(E/E_o)^4$ where subscript "o" differentiates the amplitude of electric field of the incident plane wave used, from the surface-enhanced value at the location of the emitter. The enhancement of the local intensity near a metal structure given by $(E/E_o)^2$ indicates the increase in probability of the excitation of emitters. But for the power-4 rule to be valid in general, we have to infer an additional enhancement of emission by the same factor. We ignore the difference between excitation and emission energies in its following interpretation, as this rule is applicable only when this difference in energies is insignificant compared to the width of the plasmon resonance. Neighborhood of an absorbing body includes evanescent fields, and this factor of near-field enhancement $(E/E_o)^2$ also represents the cumulative increase in radiative and
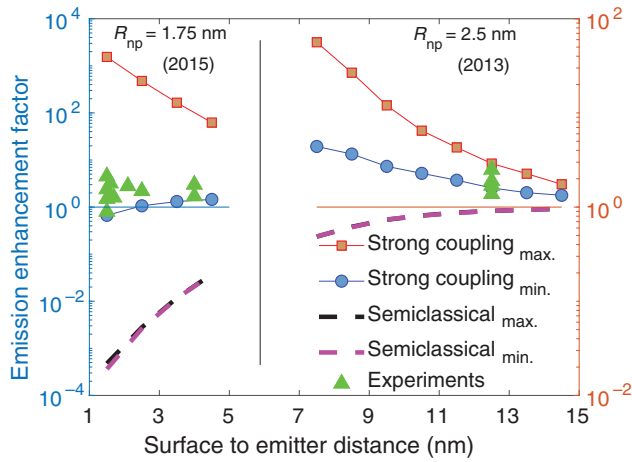
FIG. 4. Comparison of theoretical results and observed photo-luminescence: the minimum and maximum gains predicted are given by quantum efficiency and power radiated, normalized by the values of the isolated emitter; note log scale in the Y axis. For short distances 1–5 nm, experimental data [48] is for gold nanoparticles of radius 1.75 nm and the peak emission wavelength is 560 nm with $Q_o \approx 0.33$. For larger distances (7–15 nm) on the right side of the figure, four experimental data points at a mean distance of 12.5 nm [13] are for gold nanoparticles of radius 2.5 nm and a peak emission wavelength of 560 nm with $Q_o \approx 0.06$.
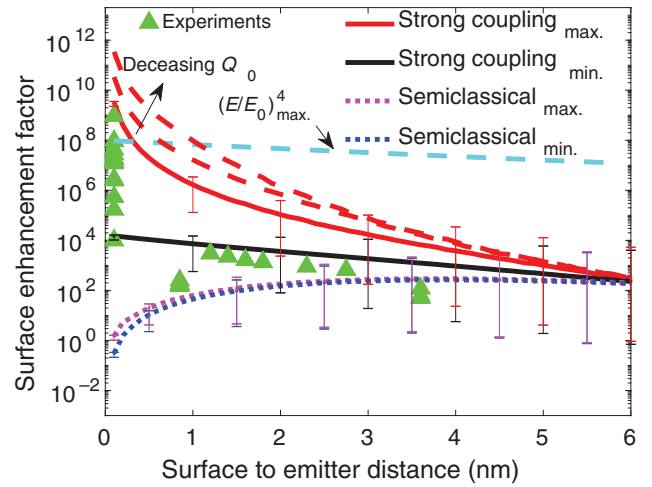
FIG. 5. Comparison of theoretical results and observed SERS: the minimum and maximum gains predicted are given by quantum efficiency and power radiated, normalized by the values of the isolated emitter and also scaled by the excitation enhancement $(E/E_o)^2$; note log scale in the Y axis. Relative $\epsilon = -1.05 + 0.035i$ at emission wavelength for half space forming the surface. Error bars placed alternately for conventional and nonlocal theories reflect variations in predictions using near-field enhancements by 2- to 50-nm-size surface features, where the lines represent a 10-nm feature. While $Q_o = 0.33$ for the solid lines, the maximum predicted values are indicated as dashed red lines for smaller Q_o of 0.033 and 0.003.

nonradiative states for such a proximal emission. Thus experiments predicted by this power-4 rule demonstrate an anomalous loss of distinction between the radiative and nonradiative states for proximal emitters that are predominantly excited in SERS. Recent experiments have demonstrated enhancements that are many orders larger than predictions of this rule, thus demanding a comprehensive theory.

Figure 5 shows optimistic predictions of enhancements using conventional and proposed theories, experimental measurements of a few distance-dependent SERS measurements [17,18], and a few reported experiments without any spacers between the SERS surface and the emitters [19,21–23]. The latter are marked closest to a distance of zero where the probability of excitation is highest. We evaluate the decay rates and average fluctuations (Γ_{leak}) using a plane surface near its plasmon resonance at the emission energy (relative permittivity $\epsilon \approx -1$), and these represent realistic gold or silver surfaces used in SERS. Note that a plane surface also approximates other structures like dimers and aggregates when separation of the emitter is much smaller than the size of these larger nanostructures. Further, for both conventional and proposed theories of emission, we add a near-field enhancement of excitation due to nano features ranging in size from 2 to 50 nm marked by error bars, with the maximum relative intensity of excitation possible in realistic nanostructures, i.e., the maximum $(E/E_o)^2$ at the surface is assumed

to be 10^4. Nevertheless, note that the very large enhancements observed are prohibited in the conventional semiclassical theory while all experiments are within the predicted range of the proposed theory. Predictions of off-resonant emission to account for some SERS measurements being away from plasmon resonance, and a comparison of the quasistatic solutions, are relegated to the Supplemental Material [47].

Note that observed Raman enhancements can be many orders of magnitude larger compared to the enhancements of fluorescence and photoluminescence, due to three primary reasons. Firstly, exciting and emission energies are not far separated in SERS and are typically close to the plasmon resonance, thus maximizing both near-field enhancements and the modified density of radiative states proposed here. Secondly, the theoretical limit of maximum enhancement possible due to a continuous excitation is not relevant to fluorescence and photoluminescence emitters, as they bleach when excited with strong radiation. This is also evident from simultaneous Raman and photoluminescence measurements where the near-field enhancement plays a negligible role [55]. Thirdly, Raman emissions have significantly lower efficiencies Q_o, and thus have a larger increase in efficiency due to effective radiative states of metal added in the strong matter-coupling regime. Note that the weak matter-coupling

approximation does not significantly add to radiative states in such cases.

Overall, the proposed theory of the density of optical states removes the large divergence observed in measured enhancements of Raman signals over many decades, and is also supported by more recent experiments of photoluminescence and fluorescence near metal nanoparticles of limiting small dimensions. While our detailed evaluations showing this effect involve dynamics of strong coupling, our alternative elucidation that involves tunneling out of photons from an absorbing nanostructure coupled to the emitter by its evanescent field, is also relevant. Further sensitive experiments may firmly establish the full theory defining the density of optical states, especially in the strong matter-coupling regime. This effect can broadly impact applications in light generation, optical sensing, and radiative heat transfer.

APPENDIX A: METHODS

To evaluate the required Green dyads, consider an emitter located at $\mathbf{r_o}$ interacting with a nanostructure or inhomogeneous matter in general, where the permittivity is a function of $\mathbf{r}$. The dyadic Green function describing this interaction in a medium of isotropic permitivitty $\epsilon(r)$ is the solution of

$$\nabla \times \nabla \times \mathbf{G}(\mathbf{r}, \mathbf{r_o}; \omega) - \epsilon(\mathbf{r}; \omega)k^2\mathbf{G}(\mathbf{r}, \mathbf{r_o}; \omega) = \mathbf{I}\delta(\mathbf{r} - \mathbf{r_o}),$$
(A1)

where $\mathbf{I}$ is a unit dyad, the wave number $k = \omega/c$, and $\delta(\mathbf{r} - \mathbf{r_o})$ represents a point source.

The above equation has no analytical solutions in general, and a quasistatic solution in the long-wavelength limit has been typically preferred. But this may result in significant errors, especially in its underestimation of nonradiative decay rates in metal nanostructures. Hence, one has to resort to more computationally intensive full-wave approaches to include retardation for finite wavelengths. We use the more efficient Sommerfeld integral solutions [56–58] to compute the retarded wave image dyadic for a surface in the near field (for the results in Fig. 5). A different approach used for the metal nano spheres discussed in Figs. 2–4, is discretization of the nanostructure into very small dipole granules. These two methods to evaluate the dyadic Green tensors for the corresponding problems are described separately. In the results presented in this work, $|\text{Re}(\Sigma)|/\omega < 0.1$, and the rotating wave approximation for the energy shifts is useful. In addition we present (in Fig. S2 within the Supplemental Material [47]) evaluations using the quasistatic approximations which are more widely used for a surface interaction. We also validate the predictions of enhancements for the metal nano spheres using the analytical single-dipole approximation (Figs. S4 and S5 within the Supplemental Material [47]).

This is to confirm that the more intensive computational approach adds only to the nonradiative contributions of the higher-order modes as expected, and indeed does not alter the conclusions of this work. Figures S6–S10 (within the Supplemental Material [47]) provide raw data of evaluated Rabi and decay rates used in Figs. 2–5 of the main manuscript.

A.1. Self-interaction dyads for emitters near arbitrary nanostructures

First we perform a discretization of the nanostructure into very small dipole granules, where interaction between any two dipole granules i, j is well approximated by the point-dipole dyadic:

$$\mathbf{G}_o(\mathbf{r_i}, \mathbf{r_j}; \omega) = \left(\mathbf{I} + \frac{\nabla\nabla}{k^2}\right)g(\|\mathbf{r_i} - \mathbf{r_j}\|),$$
(A2)

where $g(r) = e^{ikr}/4\pi r$. The green dyadic for estimating the modified self-interaction of an emitter in the presence of the nanostructure is given by [46]

$$\mathbf{G}(\mathbf{r_o}, \mathbf{r_o}; \omega) = \mathbf{G} = -\bar{G}_{ob} \cdot \bar{G}_{bb}^{-1} \cdot \bar{G}_{ob}^T,$$
(A3)

where $\bar{G}_{bb}$ is $3m \times 3m$ matrix that represents interaction among m dipole granules in the nanostructure and $\bar{G}_{ob}$ is a $3 \times 3m$ matrix that represents interaction between the emitter and each dipole granule of the nanostructure (m is in the order of $10^3 - 10^4$ for results presented in this work). Both these matrices are constructed using the 3×3 point-dipole Green dyads in Eq. (A2) for any two entities at r_j, r_i. The dipolar components can be factored from the total values, by an evaluation using a single dipole with the volume polarizability of the body. A decomposition of the metallic component Γ into its radiative and nonradiative components Γ^r and Γ^{nr} in the case of an arbitrary structure consisting dipole granules, involves factoring out the contribution of real and imaginary parts of the inverse of polarizability of granules to the dyad $\mathbf{G}$, and this was shown elsewhere [46].

A.2. Self-interaction dyads for emitters near plane surfaces

In the quasistatic case, the self-interaction tensor $\mathbf{G}$ is given by

$$\mathbf{G} = \frac{k_1^2 - k_2^2}{k_1^2 + k_2^2}\mathbf{G}^I,$$
(A4)

where k_1 and k_2 are the wave numbers for the surface and surrounding medium, respectively, and $\mathbf{G}^I$ is the image

Green dyadic given as [59]

$$
\mathbf{G}^I = \frac{1}{4\pi\epsilon_2}
\begin{bmatrix}
-\dfrac{1}{(2d)^3} & 0 & 0 \\
0 & -\dfrac{1}{(2d)^3} & 0 \\
0 & 0 & \dfrac{2}{(2d)^3}
\end{bmatrix},
$$

where d is the distance of the emitter from the surface and ϵ_2 is the permittivity of the surrounding medium. The interface separating the surrounding medium and surface is in the x-y plane and the emitter is placed at a distance d perpendicular to this plane, i.e., it is separated in the z direction.

In this long-wavelength approximation, $\mathbf{G}^I$ is real and so the imaginary and real parts of the front factor allow a decomposition into Γ^{nr} and the energy shifts. $\Gamma^{\mathrm{total}} = \Gamma^{nr} + \Gamma_o^r + \Gamma_o^{nr}$ and the contribution of the metal surface to the radiative decay is negligible in the quasistatic case. In the case of the Sommerfeld model used, $\mathbf{G}$ is given by [57]

$$
\mathbf{G} = \mathbf{S} + \frac{k_2^2}{\epsilon_2}\frac{k_1^2 - k_2^2}{k_1^2 + k_2^2}\mathbf{G}^I, \tag{A5}
$$

where components of the $\mathbf{S}$ matrix are given by Sommerfeld integrals. The Sommerfeld integrals are computed numerically using a method developed by Lager and Lytle [56–58]. $\mathbf{G}^I$ is given as [57]

$$
\mathbf{G}^I = \frac{e^{i2k_2 d}}{4\pi(2d)}
\begin{bmatrix}
-\beta & 0 & 0 \\
0 & -\beta & 0 \\
0 & 0 & \beta + \gamma
\end{bmatrix},
$$

where

$$
\beta = [1 - (2dk_2)^{-2} + (2dk_2)^{-1}i], \tag{A6}
$$

$$
\gamma = -[1 - 3(2dk_2)^{-2} + 3(2dk_2)^{-1}i]. \tag{A7}
$$

Note that this model also represents an integral over a distribution of image-dipolar sources with corresponding phases [58]. The real part of self-energy represents energy shifts and its imaginary part corresponds to decay rates

$$
\Gamma_{\mathrm{total}} = \Gamma + \Gamma_o \tag{A8}
$$

and

$$
\Gamma = \Gamma^r + \Gamma^{nr} = -2\,\mathrm{Im}\!\left(\frac{-2\pi q^2\omega}{mc^2}\mathbf{e}_o \cdot \mathbf{G} \cdot \mathbf{e}_o\right), \tag{A9}
$$

where

$$
\Gamma^r = -2\,\mathrm{Im}\!\left(\frac{-2\pi q^2\omega}{mc^2}\mathbf{e}_o \cdot \mathbf{S} \cdot \mathbf{e}_o\right),
$$

$$
\Gamma^{nr} = -2\,\mathrm{Im}\!\left(\frac{-2\pi q^2\omega}{mc^2}\mathbf{e}_o \cdot \frac{k_2^2}{\epsilon_2}\frac{k_1^2 - k_2^2}{k_1^2 + k_2^2}\mathbf{G}^I \cdot \mathbf{e}_o\right). \tag{A10}
$$

The imaginary part of Sommerfeld term $\mathbf{S}$ contributes to Γ^r and thus the contribution of the metal surface to the radiative decay is notable and its real part also contributes significantly to the energy shifts. Thus predictions of these retarded wave evaluations are marginally different from the quasistatic approximation above.

A.3. Spatial variation of near-field enhancement in SERS

To account for the generic spatial variation of near-field enhancement, $(E/E_o)^2$, due to features in a surface, we evaluate $\sqrt{(E/E_o)^4}$ where

$$
\frac{E^4}{E_o^4} = 10^8 \times \left(1 + \frac{h}{a}\right)^{-10}, \tag{A11}
$$

where h is the distance between the emitter and the feature in the metal surface, and a is the average size of features in the surface, i.e., the radius of nano islands in this case. Here the relative intensity, i.e., $(1 + h/a)^{-10}$ varying from 1 to 0 [20,24] is multiplied by a factor of 10^8, as the maximum $(E/E_o)^2$ evaluated or observed so far for various structures has been up to 10^4 [60–62].

Quantum efficiency of isolated emitters, Q_o, is assumed to be 0.33 with the effect of decreasing Q_o shown for the maximum possible enhancements. Whereas, variations with Q_o are relatively negligible for the conventional model as its radiative rates do not increase notably due to the metal surface. We use a silver surface and an imaginary surrounding medium with refractive index of 3.5 to tune the surface plasmon resonance to a free-space wavelength of 550 nm. Silver has a permitivitty of $-12.93 + 0.428i$ at 550 nm, and with surrounding medium of refractive index 3.5, the relative permittivity reduces to $-1.056 + 0.035i$ satisfying the Fröhlich condition for surface plasmon resonance.

In Fig. 5, solid and dotted lines show results of proposed theory and conventional theory, respectively, for 10-nm (diameter) nano islands. Error bars show the deviation of the results on varying the size of nano islands from 2 to 50 nm. The upper end of error bars represent results for nano islands of 50-nm size while lower ends represent 2-nm nano islands. Green triangles are from experiments performed by others [17–19,21–23]. Distance-dependent measurements are from Figs. 5, 6, and 7 in Ref. [17], and Figs. 1 and 2 in Ref. [18]. In Fig. 2 of Ref. [18], the normalized SERS enhancement factor was provided and "1"

in that figure represents a gain of 3000 (the largest gain in Fig. 1 thereof). Other experimental measurements without any spacer between SERS substrate and emitter are plotted at a near-zero distance [19,21–23].

APPENDIX B: SIZE EFFECTS

In this section, first we plot the ratio of Rabi frequency ($\Delta E/\hbar$) and decay rate (Γ) in a metal particle of varying sizes (Figs. 6 and 7), along with the ratio of nonradiative and radiative decays (Γ^{nr} and Γ^{r}). Note that (i) a larger ratio of nonradiative rate to radiative rate, and (ii) a larger factor exp(-$\hbar\Gamma/\Delta E$), determines the degree of divergence of observations from the predictions of weak matter-coupling approximation. Variation of both in a logarithmic scale are plotted for a fixed small distance of 3 nm and for a relative large distance fixed as the radius R of the metal particle. We also present the decay rates for the two different distances 3 nm and R nm as examples (Figs. 8
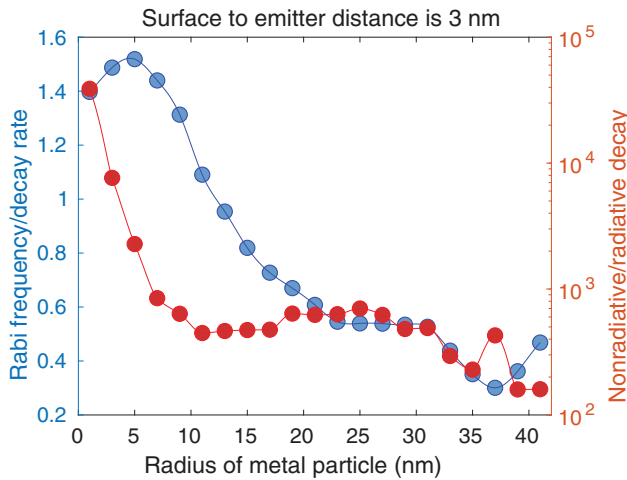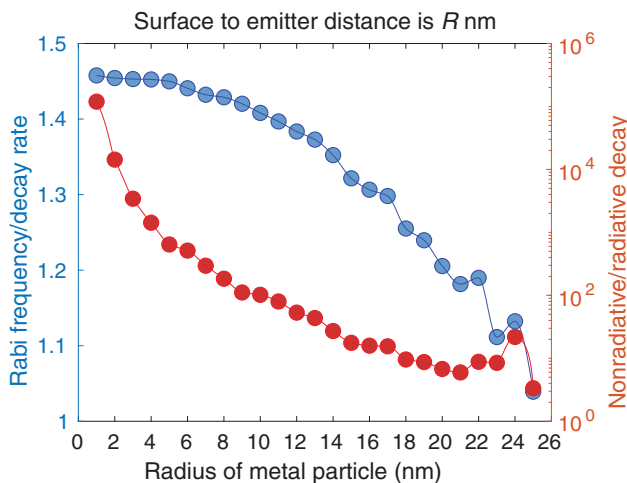

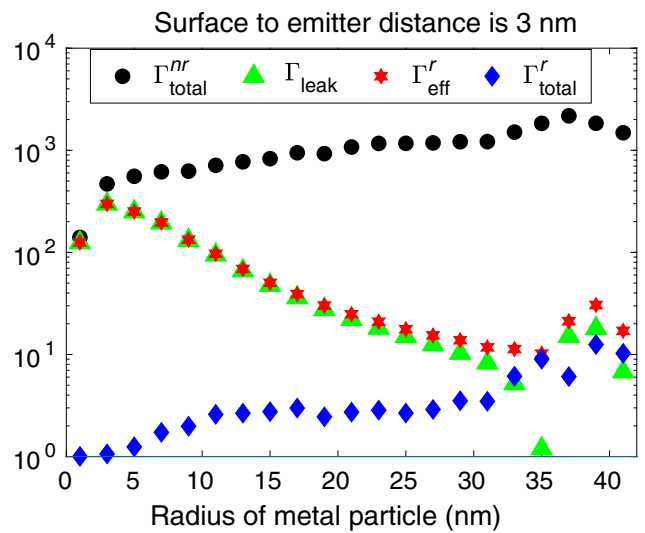FIG. 8.   Decay rates in the metal particle.

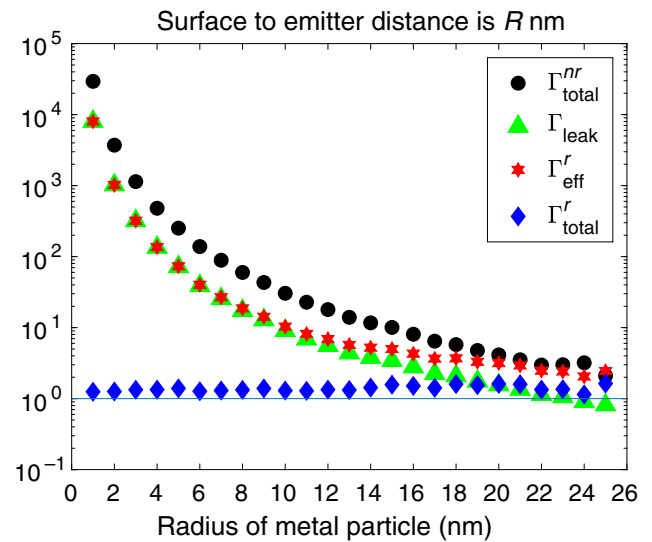FIG. 6.   Ratios indicating size effect of the metal particle.

FIG. 9.   Decay rates in the metal particle.

and 9). All decay rates are normalized by the radiative rate of the isolated emitter and are unitless. These plots provide insight into the strong coupling effects and the size of metal particles. All the above cases represent gold nanoparticles with a surrounding medium of refractive index 1.5, and at a free-space wavelength of 560 nm.

FIG. 7.   Ratios indicating size effect of the metal particle.

[1] E. M. Purcell, Resonance absorption by nuclear magnetic moments in a solid, Phys. Rev. **69**, 681 (1946).

[2] K. H. Drexhage, Influence of a dielectric interface on fluorescence decay time, J. Luminescence **1**, 693 (1970).

[3] S. Kühn, U. Håkanson, L. Rogobete, and V. Sandoghdar, Enhancement of Single-Molecule Fluorescence using a Gold Nanoparticle as an Optical Nanoantenna, Phys. Rev. Lett. **97**, 017402 (2006).

[4] P. Bharadwaj and L. Novotny, Spectral dependence of single molecule fluorescence enhancement, Opt. Exp. **15,** 14266 (2007).

[5] D. Cheng and Q. H. Xu, Separation distance dependent fluorescence enhancement of fluorescein isothiocyanate by silver nanoparticles, Chem. Commun. 248 (2007).

[6] D. Kim, H. Yokota, T. Taniguchi, and M. Nakayama, Precise control of photoluminescence enhancement and quenching of semiconductor quantum dots using localized surface plasmons in metal nanoparticles, J. Appl. Phys. **114,** 154307 (2013).

[7] E. Dulkeith, A. C. Morteani, T. Niedereichholz, T. A. Klar, J. Feldmann, S. A. Levi, F. C. J. M. Van Veggel, D. N. Reinhoudt, M. Möller, and D. I. Gittins, Fluorescence Quenching of Dye Molecules Near Gold Nanoparticles: Radiative and Nonradiative Effects, Phys. Rev. Lett. **89,** 203002 (2002).

[8] E. Dulkeith, M. Ringler, T. A. Klar, J. Feldmann, A. Munoz Javier, and W. J. Parak, Gold nanoparticles quench fluorescence by phase induced radiative rate suppression, Nano Lett. **5,** 585 (2005).

[9] A. F. Koenderink, On the use of Purcell factors for plasmon antennas, Opt. Lett. **35,** 4208 (2010).

[10] L. N. Tripathi, M. Praveena, and J. K. Basu, Plasmonic tuning of photoluminescence from semiconducting quantum dot assemblies, Plasmonics **8,** 657 (2013).

[11] K. A. Kang, J. Wang, J. B. Jasinski, and S. Achilefu, Fluorescence manipulation by gold nanoparticles: From complete quenching to extensive enhancement, J. Nanobiotechnol. **9,** 16 (2011).

[12] G. Schneider, G. Decher, N. Nerambourg, R. Praho, M. H. V. Werts, and M. Blanchard-Desce, Distance-dependent fluorescence quenching on gold nanoparticles ensheathed with layer-by-layer assembled polyelectrolytes, Nano Lett. **6,** 530 (2006).

[13] M. Haridas, J. K. Basu, A. K. Tiwari, and M. Venkatapathi, Photoluminescence decay rate engineering of CDSE quantum dots in ensemble arrays embedded with gold nano-antennae, J. Appl. Phys. **114,** 064305 (2013).

[14] M. Haridas, L. N. Tripathi, and J. K. Basu, Photoluminescence enhancement and quenching in metal-semiconductor quantum dot hybrid arrays, Appl. Phys. Lett. **98,** 27 (2011).

[15] M. Haridas, J. K. Basu, D. J. Gosztola, and G. P. Wiederrecht, Photoluminescence spectroscopy and lifetime measurements from self-assembled semiconductor-metal nanoparticle hybrid arrays, Appl. Phys. Lett. **97,** 189 (2010).

[16] M. Haridas and J. K. Basu, Controlled photoluminescence from self-assembled semiconductor–metal quantum dot hybrid array films, Nanotechnol. **21,** 415202 (2010).

[17] G. J. Kovacs, R. O. Loutfy, P. S. Vincett, C. Jennings, and R. Aroca, Distance dependence of SERS enhancement factor from Langmuir-Blodgett monolayers on metal island films: Evidence for the electromagnetic mechanism, Langmuir **2,** 689 (1986).

[18] Q. Ye, J. Fang, and L. Sun, Surface-enhanced Raman scattering from functionalized self-assembled monolayers. 2. Distance dependence of enhanced Raman scattering from an azobenzene terminal group, J. Phys. Chem. B **101,** 8221 (1997).

[19] A. D. McFarland, M. A. Young, J. A. Dieringer, and R. P. Van Duyne, Wavelength-scanned surface-enhanced Raman excitation spectroscopy, J. Phys. Chem. B **109,** 11279 (2005).

[20] J. A. Dieringer, A. D. McFarland, N. C. Shah, D. A. Stuart, A. V. Whitney, C. R. Yonzon, M. A. Young, X. Zhang, and R. P. Van Duyne, Surface enhanced Raman spectroscopy: New materials, concepts, characterization tools, and applications, Faraday Discussions **132,** 9 (2006).

[21] D. Wang, W. Zhu, M. D. Best, J. P. Camden, and K. B. Crozier, Wafer-scale metasurface for total power absorption, local field enhancement and single molecule Raman spectroscopy, Sci. Rep. **3,** 2867 (2013).

[22] A. M. Gabudean, M. Focsan, and S. Astilean, Gold nanorods performing as dual-modal nanoprobes via metal-enhanced fluorescence (MEF) and surface-enhanced Raman scattering (SERS), J. Phys. Chem. C **116,** 12240 (2012).

[23] V. G. Ivanov, N. D. Todorov, L. S. Petrov, T. Ritacco, M. Giocondo, and E. S. Vlakhov, in *Journal of Physics: Conference Series* (IOP Publishing, London, 2016), Vol. 764, p. 012023.

[24] B. J. Kennedy, S. Spaeth, M. Dickey, and K. T. Carron, Determination of the distance dependence and experimental effects for modified SERS substrates based on self-assembled monolayers formed using alkanethiols, J. Phys. Chem. B **103,** 3640 (1999).

[25] E. C. Le Ru and P. G. Etchegoin, Rigorous justification of the E^4 enhancement factor in surface enhanced Raman spectroscopy, Chem. Phys. Lett. **423,** 63 (2006).

[26] M. Moskovits, Persistent misconceptions regarding SERS, Phys. Chem. Chem. Phys. **15,** 5301 (2013).

[27] G. Sun, J. B. Khurgin, and D. P. Tsai, Comparative analysis of photoluminescence and Raman enhancement by metal nanoparticles, Opt. Lett. **37,** 1583 (2012).

[28] D. P. Fromm, A. Sundaramurthy, A. Kinkhabwala, P. J. Shuck, G. S. Kino, and W. E. Moerner, Exploring the chemical enhancement for surface-enhanced Raman scattering with Au bowtie nanoantennas, J. Chem. Phys. **124,** 61101 (2006).

[29] B. Sharma, R. R. Frontiera, A. I. Henry, E. Ringe, and R. P. Van Duyne, SERS: Materials, applications, and the future, Materials Today **15,** 16 (2012).

[30] K. Kneipp, Chemical contribution to SERS enhancement: An experimental study on a series of polymethine dyes on silver nanoaggregates, J. Phys. Chem. C **120,** 21076 (2016).

[31] J. M. Raimond, P. Goy, M. Gross, C. Fabre, and S. Haroche, Statistics of Millimeter-Wave Photons Emitted by a Rydberg-Atom Maser: An Experimental Study of Fluctuations in Single-Mode Superradiance, Phys. Rev. Lett. **49,** 1924 (1982).

[32] Y. Zhu, D. J. Gauthier, S. E. Morin, Q. Wu, H. J. Carmichael, and T. W. Mossberg, Vacuum Rabi splitting as a feature of linear-dispersion theory: Analysis and experimental observations, Physical Review Letters **64,** 2499 (1990).

[33] A. Boca, R. Miller, K. M. Birnbaum, A. D. Boozer, J. McKeever, and H. J. Kimble, Observation of the Vacuum Rabi Spectrum for One Trapped Atom, Phys. Rev. Lett. **93,** 233603 (2004).

[34] T. Yoshie, A. Scherer, J. Hendrickson, G. Khitrova, H. M. Gibbs, G. Rupper, C. Ell, O. B. Shchekin, and D. G. Deppe, Vacuum Rabi splitting with a single quantum dot in a photonic crystal nanocavity, Nature **432,** 200 (2004).

[35] F. Bernardot, P. Nussenzveig, M. Brune, J. M. Raimond, and S. Haroche, Vacuum Rabi splitting observed on a microscopic atomic sample in a microwave cavity, EPL **17,** 33 (1992).

[36] J. Bellessa, C. Bonnand, J. C. Plenet, and J. Mugnier, Strong Coupling between Surface Plasmons and Excitons in an Organic Semiconductor, Phys. Rev. Lett. **93,** 036404 (2004).

[37] G. Zengin, M. Wersäll, T. J. Nilsson, S. Antosiewicz, M. Kall, and T. Shegai, Realizing Strong Light-Matter Interactions between Single-Nanoparticle Plasmons and Molecular Excitons at Ambient Conditions, Phys. Rev. Lett. **114,** 157401 (2015).

[38] P. M. Adam, L. Salomon, F. de Fornel, and J. P. Goudonnet, Determination of the spatial extension of the surface-plasmon evanescent field of a silver film with a photon scanning tunneling microscope, Phys. Rev. B **48,** 2680 (1993).

[39] A. J. Meixner, M. A. Bopp, and G. Tarrach, Direct measurement of standing evanescent waves with a photon-scanning tunneling microscope, Appl. Opt. **33,** 7995 (1994).

[40] J. D. Baena, L. Jelinek, R. Marqués, and F. Medina, Near-perfect tunneling and amplification of evanescent electromagnetic waves in a waveguide filled by a metamaterial: Theory and experiments, Phys. Rev. B **72,** 075116 (2005).

[41] J. J. Loomis and H. J. Maris, Theory of heat transfer by evanescent electromagnetic waves, Phys. Rev. B **50,** 18517 (1994).

[42] S. Rytov, *Theory of Electrical Fluctuations and Thermal Radiation* (Academy of Sciences Press, Moscow, 1953).

[43] M. K. Parikh and F. Wilczek, Hawking Radiation as Tunneling, Phys. Rev. Lett. **85,** 5042 (2000).

[44] V. N. Pustovit and T. V. Shahbazyan, Plasmon-mediated superradiance near metal nanostructures, Phys. Rev. B **82,** 075429 (2010).

[45] C. Van Vlack, P. T. Kristensen, and S. Hughes, Spontaneous emission spectra and quantum light-matter interactions from a strongly coupled quantum dot metal-nanoparticle system, Phys. Rev. B **85,** 075303 (2012).

[46] M. Venkatapathi, Collective eigenstates of emission in an n-entity heterostructure and the evaluation of its green tensors and self-energy components, J. Opt. Soc. Am. B **31,** 3153 (2014).

[47] See Supplemental Material at http://link.aps.org/supplemental/10.1103/PhysRevApplied.11.054002 for additional information on cited experimental results and simulated data.

[48] M. Praveena, A. Mukherjee, M. Venkatapathi, and J. K. Basu, Plasmon-mediated emergence of collective emission and enhanced quantum efficiency in quantum dot films, Phys. Rev. B **92,** 235403 (2015).

[49] V. N. Pustovit and T. V. Shahbazyan, Cooperative Emission of Light by an Ensemble of Dipoles Near a Metal Nanoparticle: The Plasmonic Dicke Effect, Phys. Rev. Lett. **102,** 077401 (2009).

[50] E. O. Potma and D. A. Wiersma, Exciton superradiance in aggregates: The effect of disorder, higher order exciton-phonon coupling and dimensionality, J. Chem. Phys. **108,** 4894 (1998).

[51] M. Gross and S. Haroche, Superradiance: An essay on the theory of collective spontaneous emission, Phys. Rep. **93,** 301 (1982).

[52] M. Scheibner, T. Schmidt, L. Worschech, A. Forchel, G. Bacher, T. Passow, and D. Hommel, Superradiance of quantum dots, Nat. Phys. **3,** 106 (2007).

[53] A. Goban, C. L. Hung, J. D. Hood, S. P. Yu, J. A. Muniz, O. Painter, and H. J. Kimble, Superradiance for Atoms Trapped Along a Photonic Crystal Waveguide, Phys. Rev. Lett. **115,** 063601 (2015).

[54] M. L. Juan, C. Bradac, B. Besga, G. Molina-Terriza, and T. Volz, Cooperatively enhanced dipole forces from artificial atoms in trapped nanodiamonds, Nat. Phys. **13,** 241 (2017).

[55] M. Kawai, A. Yamamoto, N. Matsuura, and Y. Kanemitsu, Energy transfer in mixed CdSe and Au nanoparticle monolayers studied by simultaneous photoluminescence and Raman spectral measurements, Phys. Rev. B **78,** 153308 (2008).

[56] R. J. Lytle and D. L. Lager, Numerical evaluation of Sommerfeld integrals, type Tech. Rep. (Lawrence Livermore Laboratories, 1974).

[57] R. Schmehl, B. M. Nebeker, and E. D. Hirleman, Discrete-dipole approximation for scattering by features on surfaces by means of a two-dimensional fast Fourier transform technique, J. Opt. Soc. Am. A **14,** 3026 (1997).

[58] I. Arun and M. Venkatapathi, Analysis of numerical solutions to Sommerfeld integral relation of the half-space radiator problem, Appl. Numer. Math. **106,** 79 (2016).

[59] L. Novotny and B. Hecht, *Principles of Nano-Optics* (Cambridge University Press, Cambridge, 2012).

[60] Y. Huang, L. Ma, M. Hou, J. Li, Z. Xie, and Z. Zhang, Hybridized plasmon modes and near-field enhancement of metallic nanoparticle-dimer on a mirror, Sci. Rep. **6,** 30011 (2016).

[61] G. Pellegrini, M. Celebrano, M. Finazzi, and P. Biagioni, Local field enhancement: Comparing self-similar and dimer nanoantennas, J. Phys. Chem. C **120,** 26021 (2016).

[62] G. C. Schatz, M. A. Young, and R. P. Van Duyne, in *Surface-Enhanced Raman Scattering* (Springer, New York, 2006), p. 19.